

Electronic supplementary information

Polarization-resolved single-molecule tracking reveals strange dynamics of fluorescent tracers through a deep rubbery polymer network

Jaladhar Mahato, Sukanya Bhattacharya, Dharmendar K. Sharma[‡], and Arindam Chowdhury*.

Department of Chemistry, Indian Institute of Technology Bombay, Powai, Mumbai 400076, India

[‡]Present address: Department of Chemistry, Maulana Azad National Institute of Technology, Bhopal, 462003, India

*Email: arindam@chem.iitb.ac.in

Supplementary Text

Materials and Methods

Materials: Polyvinylpyrrolidone (PVP) (MW 40 000, Sigma Aldrich) was used as received. Rhodamine 6G (Rh6G) (Radiant Dyes, Germany) was used as the fluorescent probe. Glass coverslips (No. 1, Corning, USA) were used as a substrate to spin-cast the polymer from aqueous solution (using MilliQ water).

Sample Preparation: The thin film of PVP sparsely dispersed with Rh6G was prepared as described previously.¹ In Brief, glass coverslips were cleaned by sonication for 15 min using the Piranha solution, then with 2 M NaOH followed by washing using Milli Q water. A ~200nm thick polymer film is prepared to remove the interfacial effects, using the method employed by Liu *et al.*² First, 20 μ L PVP solution was spin-coated over the precleaned glass coverslip followed by 20 μ L of ~300 pM solution of Rh6G premixed with PVP. Finally, 20 μ L of PVP solution was spin-casted on top of it. Each of the steps is performed at 2000 rpm for 1 min, and the concentration of PVP was maintained at 2 mg/mL in each solution. The samples were annealed at ~400K for 2h under evacuated conditions to ensure residual solvent removal. The film thickness was found to be ~200 \pm 30 nm using both ellipsometry and atomic force microscopy. A home-built enclosed chamber was mounted on top of the sample stage to control

the relative humidity (RH) within the thin film by regulating the flow of argon gas bubbled through water (**Fig. S2**, inset). The PVP thin film was exposed to a fixed ambient RH for 30 min before data collection and held constant during the data acquisition.

Polarization Resolved SM Fluorescence Microscopy: Single-molecule (SM) imaging has been performed in a home-built polarization-resolved epifluorescence setup based on an inverted microscope (Nikon TE200U); the details can be found elsewhere.³ A simple schematic of the setup is presented in **Fig. S2**. Briefly, a continuous-wave 532nm DPSS (LaserGlow, 50 mW) laser light has been expanded using a beam expander (BE) and polarized circularly by a $\lambda/4$ wave plate and subsequently focused at the back focal plane (BFP) of an oil immersion objective (Nikon, 1.49 NA, 60X TIRF) to illuminate (wide-field mode) the sample kept in the control environment. The excitation power was controlled using neutral density filters (NDF) and maintained at ~ 0.5 kW/cm², measured after the objective. The emission from the sample was collected by the same objective and passed through an appropriate dichroic mirror (Semrock, Di01-R532) and a sharp notch filter (Semrock, LP03-532RU) before imaging in an air-cooled (-25 °C) interline CCD camera (DVC-1412AM). The fluorescence intensity from an SM probe is spread over more than the $\sim 2.5 \times 2.5$ pixels, the fwhm of the diffraction-limited spot. A polarizing beam displacing Wollaston prism (ThorLabs BD27) was placed in between the relay lens, which separates the emission intensity into two mutually orthogonal polarized emission components (S- and P-). The CCD camera position and the Wollaston prism were maintained to detect the two polarized emission channels simultaneously in two circular (diameter ~ 8 μ m) fields of views (FOVs). All the polarization-resolved movies (16-bit format) were collected with data acquisition (τ_{exp}) timescale at 10 Hz and measurements were performed at 295K. The DVC View image acquisition software was used to collect polarization-resolved movies, and ImageJ (NIH) was subsequently used for SM image analysis.

PR-SMT data extraction: S- and P- polarized-resolved channels were obtained by cropping the acquired movies via visual inspection and careful pixel-by-pixel overlay of the two FOVs (**Fig. 2a**). The background subtraction has been done using ImageJ with a rolling-ball radius of 30 pixels of these movies, ensuring that the possibility of error due to the background is minimized. Spatially well separated (> 0.5 μ m) diffraction-limited spots (such as M1 and M2 in **Fig. 2b**) from the different regions of interest (ROI) were chosen from S- and P- polarized-resolved channels. The intensity-weighted addition ($I_T(t) = I_S(t) + I_P(t)$) of these two polarized movies have been performed at each pixel location. This movie is used for super-localization (5×5 pixels around the PSF). Sequential snapshots of three SMs have been shown

in **Fig. S3**. It has to be mention that only those emission spots were chosen from the combined movie where the signal to background ratio (SBR) is >3 and had fewer photoblinking events. A script written in MATLAB (The Mathworks, Inc., and Natick, Massachusetts) was used to super-localize the position ($\{x(t), y(t)\}$) in each frame of the SM images using the centroid method.

$$x(t) = \frac{\sum_{i=1}^n \sum_{j=1}^m x_i(t) \cdot I_{ij}(t)}{\sum_{i=1}^n \sum_{j=1}^m I_{ij}(t)}; y(t) = \frac{\sum_{i=1}^n \sum_{j=1}^m y_j(t) \cdot I_{ij}(t)}{\sum_{i=1}^n \sum_{j=1}^m I_{ij}(t)}$$

Here (x_i, y_j) is the coordinate of the pixel on the x and y -axis, respectively and $I_{ij}(t)$ is the intensity on that pixel at frame t . The classification of the obtained super-resolved trajectory into different categories (Cat) has been performed using the radius of gyration (R_g) which was calculated by a method employed by Bohn *et al.*⁴ –

$$R_g = \sqrt{R_1^2 + R_2^2}$$

where R_1 and R_2 are the major and minor eigenvalues respectively of the radius of gyration tensor, \hat{R} .

$$\hat{R} = \begin{pmatrix} \sum_{i=0}^n \sqrt{(x_i - \langle x \rangle)^2} & \sum_{i=0}^n \sqrt{|(x_i - \langle x \rangle)| \cdot |(y_i - \langle y \rangle)|} \\ \sum_{i=0}^n \sqrt{|(x_i - \langle x \rangle)| \cdot |(y_i - \langle y \rangle)|} & \sum_{i=0}^n \sqrt{(y_i - \langle y \rangle)^2} \end{pmatrix}$$

The emission intensity as a function of acquisition time at the two polarized channels, $I_s(t)$ and $I_p(t)$, is calculated by incorporating the S - and P - polarized movies in the same script where counts are summed from only those pixels which were used for super-localization ($\{x(t), y(t)\}$). The reduced linear dichroism $LD(t)$ was computed from these $I_s(t)$ and $I_p(t)$

$$LD(t) = \frac{\{I_s(t) - I_p(t)\}}{\{I_s(t) + I_p(t)\}}$$

which in turn provide the in-plane dynamic orientation, $\phi(t)$, of SM dipoles, $LD(t) = \cos 2\phi(t)$. Our LD measurements are in tune with other prior measurements for SM reorientational dynamics.⁵ The offset of LD has been corrected for each Wollaston prism angle before further analysis. While $LD(t)$ provide in-plane dynamic orientation of SM dipoles; SM super-localization provide the coordinates ($\{x(t), y(t)\}$) of the dipole at the same time. SM

trajectory/scatter plot is generated from these coordinates ($\{x(t), y(t)\}$) and $LD(t)$ in MATLAB (**Fig. 3, S4, S5 and S11**). The left y-axis represents the position ($\{x(t), y(t)\}$) and the right y-axis reorientation in terms of $LD(t)$ in the time trajectory. The x - and the y-axis in the 3D scatter plot represents the X and Y lateral translational movement and z-axis for the LD.

Error estimation in PR-SMT: For error assessment in displacements and the $LD(t)$, we performed PR imaging of SMs embedded in a glassy (dehydrated) PVP matrix for which the T_g is ~ 120 K above the measurement temperature of 295 K. Under these conditions (ambient RH $\sim 10\%$), the polymer network cavities are extremely compact and rigid, preventing even dipolar reorientation.³ **Fig. S4a** shows a 3D scatter plot of $LD(t)$ against localized positions $\{x(t), y(t)\}$ and corresponding trajectories (**Fig. S4b**) for such an Rh6G molecule (M10). The distributions of positions and LD for this probe is shown in **Fig. S4b** (inset), which reveal that M10 is located within ~ 30 nm (lateral range), with a standard deviation (σ) of ~ 8 nm. Further, consistent high magnitude of $LD(t)$ (0.65-0.55) with nominal σ (~ 0.063) point out that only dipolar wobbling ($\Delta\phi < 10^\circ$) is permissible over several seconds. To estimate the localization error (LE), we constructed position distributions ($P(q)$) of 46 such immobile SMs with SBR ranging from 2-5, which yielded a σ in localization (σ_{xy}) of ~ 13 nm (**Fig. S4c**). As a conservative estimate, we considered the LE to be ~ 40 nm ($3\sigma_{xy}$), displacement (Δq) beyond which served as an indicator for translational movement of tracers.⁶ It should be that a fixed non-rotating molecule introduces additional error while locating the dipole depending on the tilt with respect to the object plane.^{7,8} Engelhardt *et al* demonstrated that in epifluorescence microscopy, the additional error is nominal when the dipole is tilted at 0° or 90° and is maximum at 52° .⁹ Moreover, according to this article, the extra LE would not be more than 35 nm for our system, considering the sample thickness ~ 200 nm ($z = \pm 100$ nm from the focal plane). Further, the σ for LD (σ_{LD}) for the same 46 SMs was found to be ~ 0.09 (**Fig. S4c**). In contrast, translationally static single Rh6G molecules in partially hydrated PVP which undergo hindered large-angle reorientation has been reported to have a σ_{LD} of ~ 0.25 , owing to relatively slow (20-40Hz) timescale tumbling associated with frequent momentary pauses³. Therefore, for a mobile tracer, where translational motion is accompanied by facile (unobstructed) reorientation, a zero-centered unimodal $P(LD)$ with much smaller σ_{LD} is expected. Even if the inherent noise in the $LD(t)$ measurements, σ_{min} , is ~ 0.1 , an event with $|LD(t)|$ greater than 0.25 ($2.5\sigma_{min}$) can only be a consequence of either rotational immobility or very slow hindered reorientation of individual dipoles. Detection of such events in PR-SMT provides evidence of (momentary) translational immobility of SMs navigating in the rubbery polymer film.

PR-SMT data analysis: In our measurements, a displacement of greater than 40 nm ($3\sigma_{xy}$) was considered as a clear translational mobile event, referred to as the dimension of the localization error (LE). A MATLAB script was written to describe the reorientational propensity of a dipole in a displacement trajectory based on consecutive $LD(t)$ values. Since a translationally mobile dipole is associated with the fast reorientation dynamics, the $|LD|$ will have values around zero ($< 2.5\sigma_{LD}$) over time. While an orientationally fixed dipole or slowly hindered dipole will yield high $|LD|$ value except at $\theta = 45^\circ$ (see the *polarization-resolved single-molecule tracking* section of the main manuscript). However, in a spatiotemporal heterogeneous media, a dipole undergoes a diverse variety of rotational and translational dynamics and hence to account for the rotational mobility at t during the transport, $LD(t - 1)$, $LD(t)$ and $LD(t + 1)$ were taken into consideration, along with their difference, as described in the flowchart of **Fig. S7**. Translation mobility criteria were incorporated in the reorientational propensity criteria to address the dynamics within and beyond localization error for a given time point. This script decomposes the mobility of a dipole during its movement into four categories, and a color-coded temporal trajectory has been generated to visualize these events. Displacements beyond the LE with fast rotation are identified as a clear translational event and assigned green color. The event, where displacements are within the LE and associated with fixed orientation or slow hindered rotation (respect to τ_{exp}) are true authentic pauses (red), while rotation with facile reorientation is identified as the localized motion (yellow). However, an unusual event arise very rarely where displacements are beyond LE ; however the $|LD(t)| > 2.5\sigma_{LD}$ and is colored grey. We refrain from assigning the events as mobile or immobile events when $LD(t)$ is high, and the coordinate change is $\Delta q > 40\text{nm}$ and designated as unusual events to be cautious about fixed tilted orientation. Photo blinking events are and represented by white color.

Statistics of 100 SMs: The pause dwell-times, the time-intervals between consecutive pauses, and the frequency of immobile events are calculated from each SM trajectory for 100 tracers using a MATLAB script by identifying the authentic transient immobile time points in the color-coded PR-SMT trajectory. The molecules are randomly selected based on the SBR and the tracers' time length from many FOVs. The results are shown in **Fig. 5** of the main manuscript. We have truncated the x-axis for clarity, 12s for **Fig. 5c**, 5.4s for **Fig. 5d**, and excluded the immobile molecules for an extended duration (Category I) in **Fig. 5e**.

Supplementary Figures

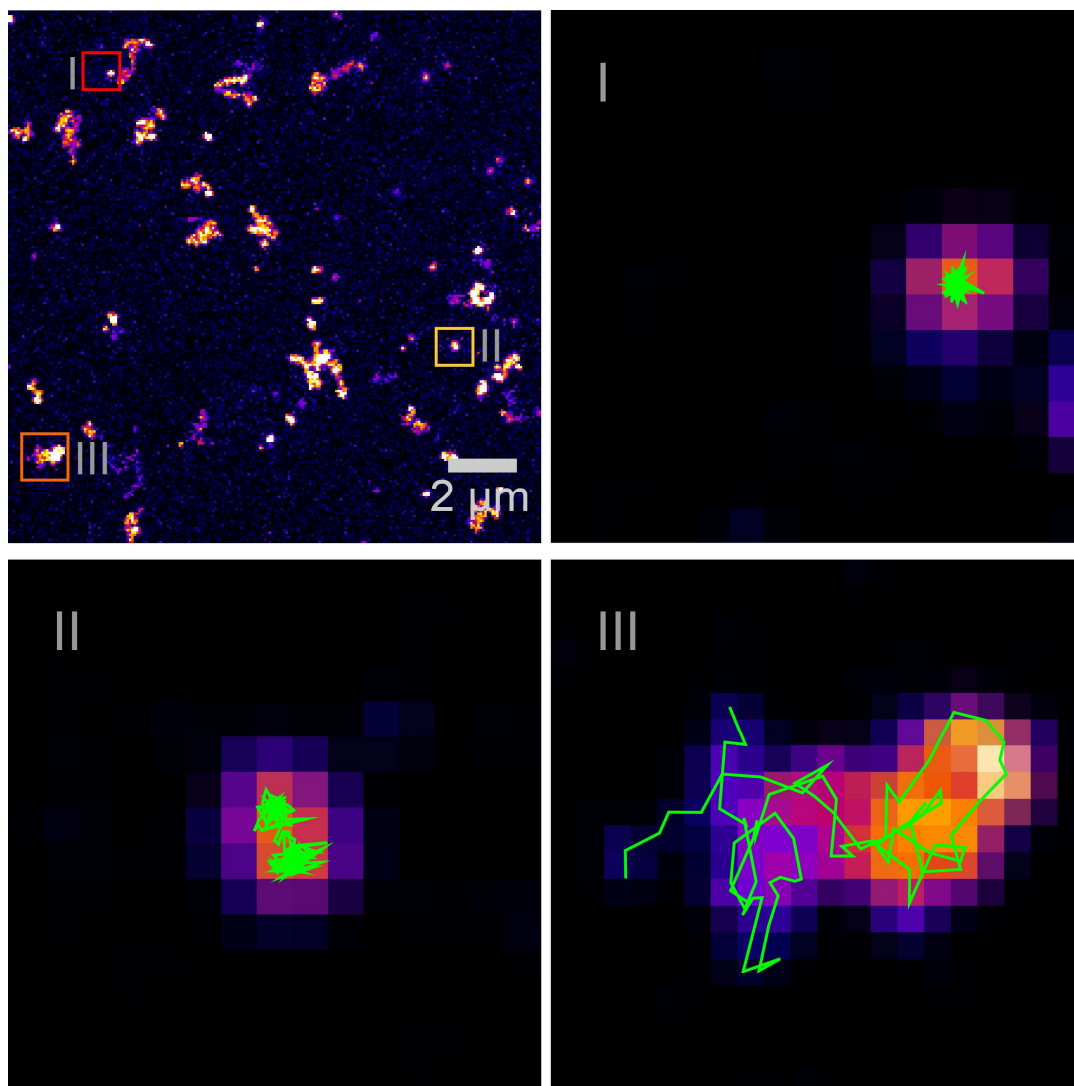


Fig. S1: Blown-up of three representative regions from the maximum projection image (Fig. 1) of Rh6G molecular probe in plasticized PVP thin films (ambient RH ~75%) showing three tracers which experience three distinct dynamic environments as quantified by the radius of gyration (R_g) trajectory.

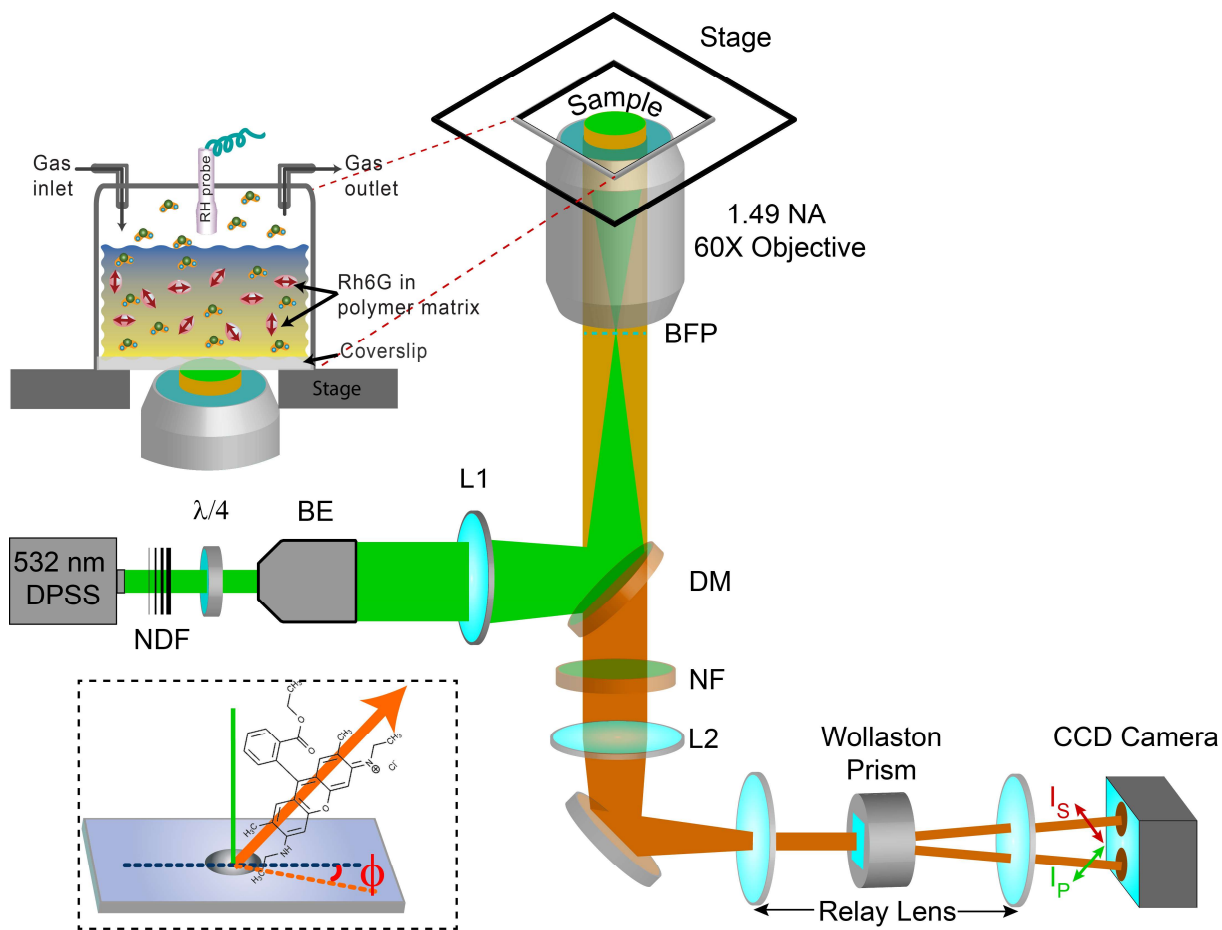


Fig. S2: Schematic of polarization-resolved SM tracking setup (details are provided in methods, SI). NDF, neutral density filter; $\lambda/4$, quarter-wave plate; L1-L2, lenses; BFP, back focal plane; DM, dichroic mirror; NF, notch filter. A Wollaston prism placed before the CCD split the emission into two orthogonal (S/P) polarizations. The inset (bottom) shows the in-plane projection for a dipole with azimuthal angle ϕ .

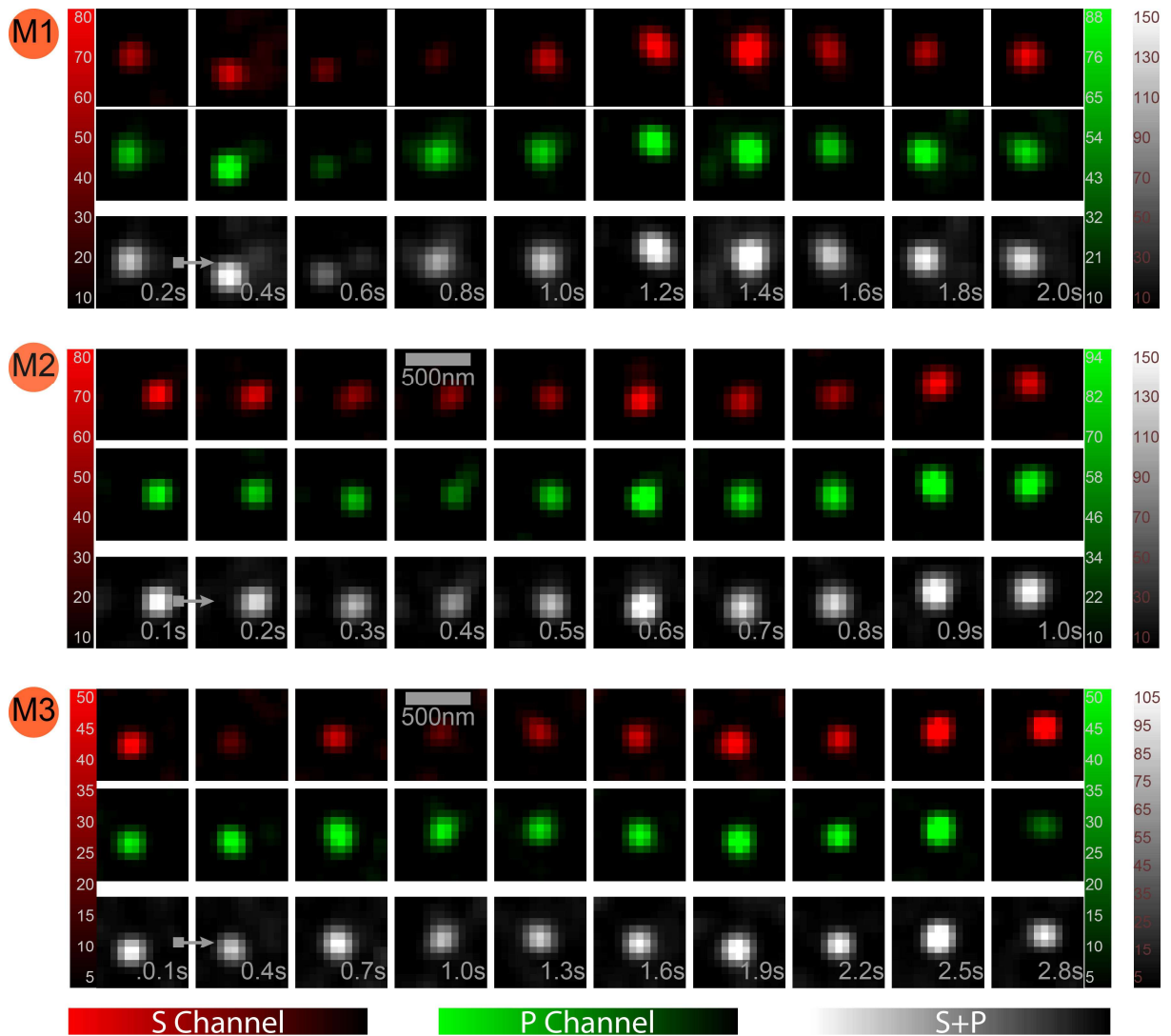


Fig. S3: Individual S-/ P- channels that are used for the quantitative pseudo-color superimposed anisotropy images, shown in Fig. 2 of the main manuscript. The intensity weighted addition of these channels employed for super-localization of position ($\{x(t), y(t)\}$). The S- and P- channels are assigned red and green color, respectively, while the intensity weighted addition image as greyscale.

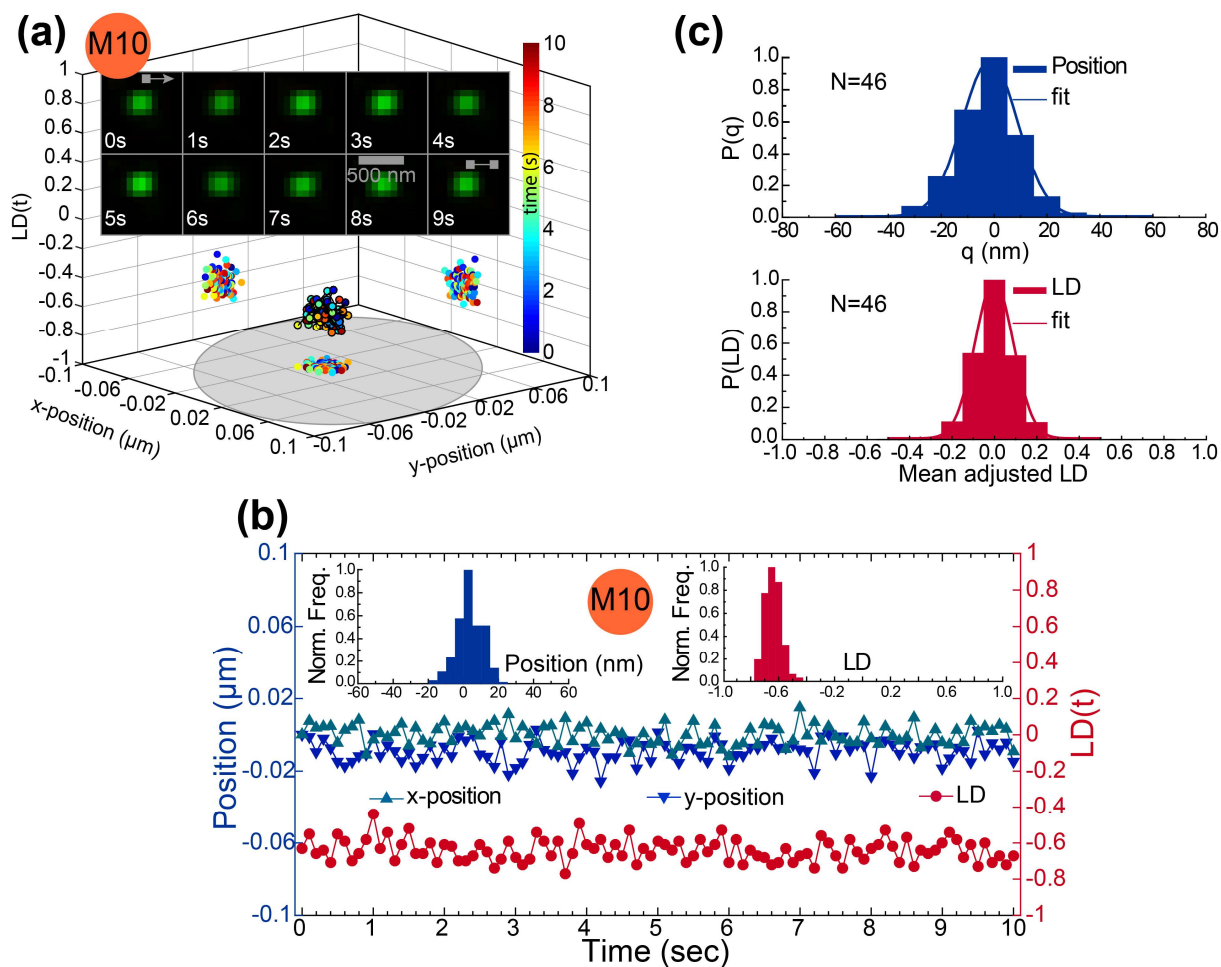


Fig. S4: (a) 3D scatter plot of localized position $\{x(t), y(t)\}$ and $LD(t)$ of one completely immobile SM (M10) within a high- T_g (rigid and compact) PVP matrix. The inset shows the pseudo-color (merged) polarization image snapshots at 1s intervals. (b) trajectories of localized positions $\{x(t), y(t)\}$, and $LD(t)$ for M10. The time-averaged distributions of position and $LD(t)$ are shown in inset. (c) Distribution of positions and $LD(t)$ for 46 immobile Rh6G molecules embedded in a high- T_g PVP film.

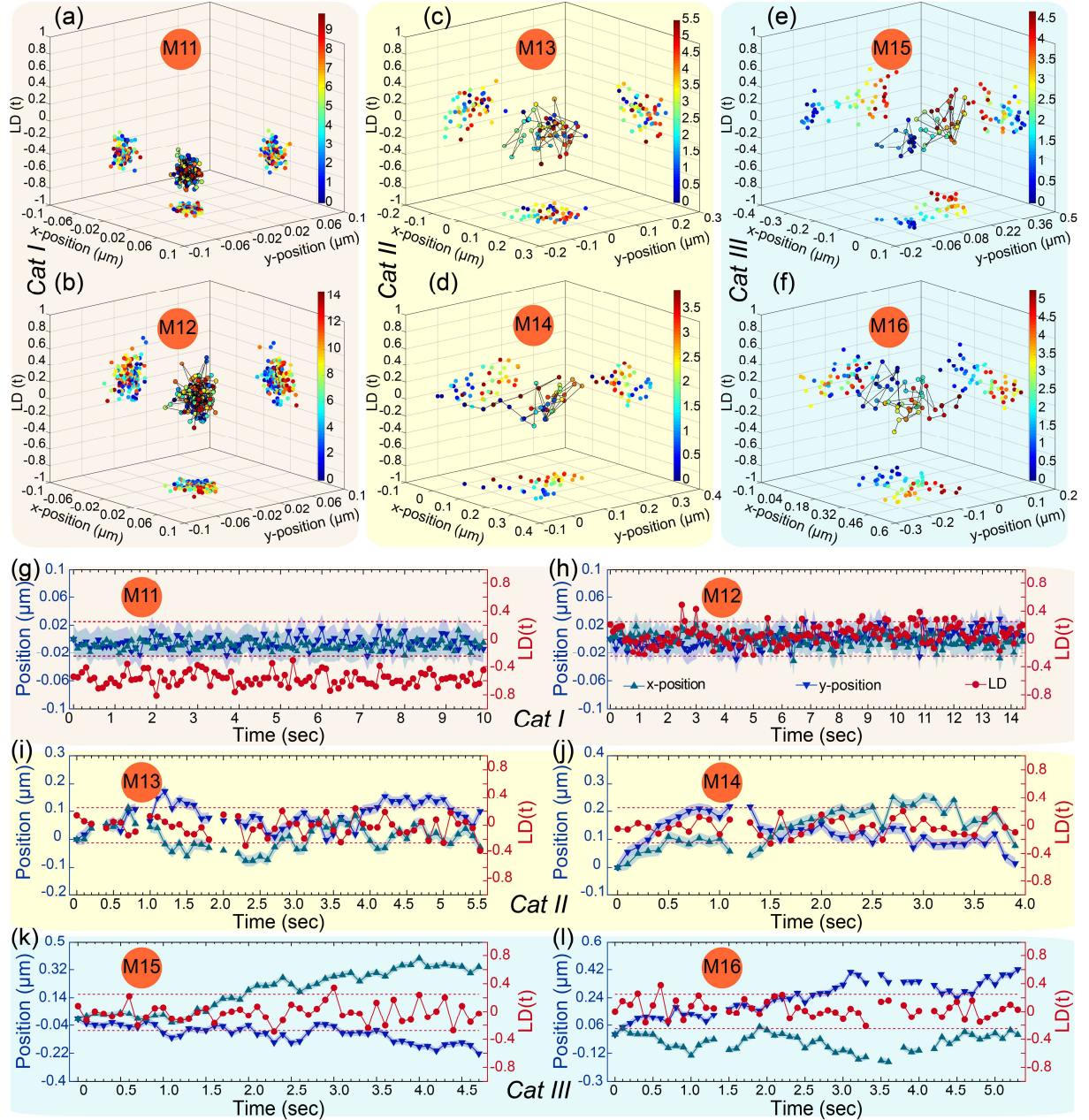


Fig. S5: Six additional representatives PR-SMT trajectories (M11-M16), two representatives from each three different dynamic categories, similar to Fig. 3 in the main manuscript. Fig. S5e-f is the scatter plot of position ($\{x(t), y(t)\}$) and $LD(t)$ and Fig. S5g-l are it's the temporal trajectories. M11- and M12 are the representative from *category I* and shown in Fig. S5 (a, b) and (g, h) while Fig. S5(c, d) and (i, j) is the scatter plot and the temporal trajectories for M13 and M14 representative of *category II* tracers. The representatives of *category III* tracers are shown in Fig. S5 (e, f) and (k, l).

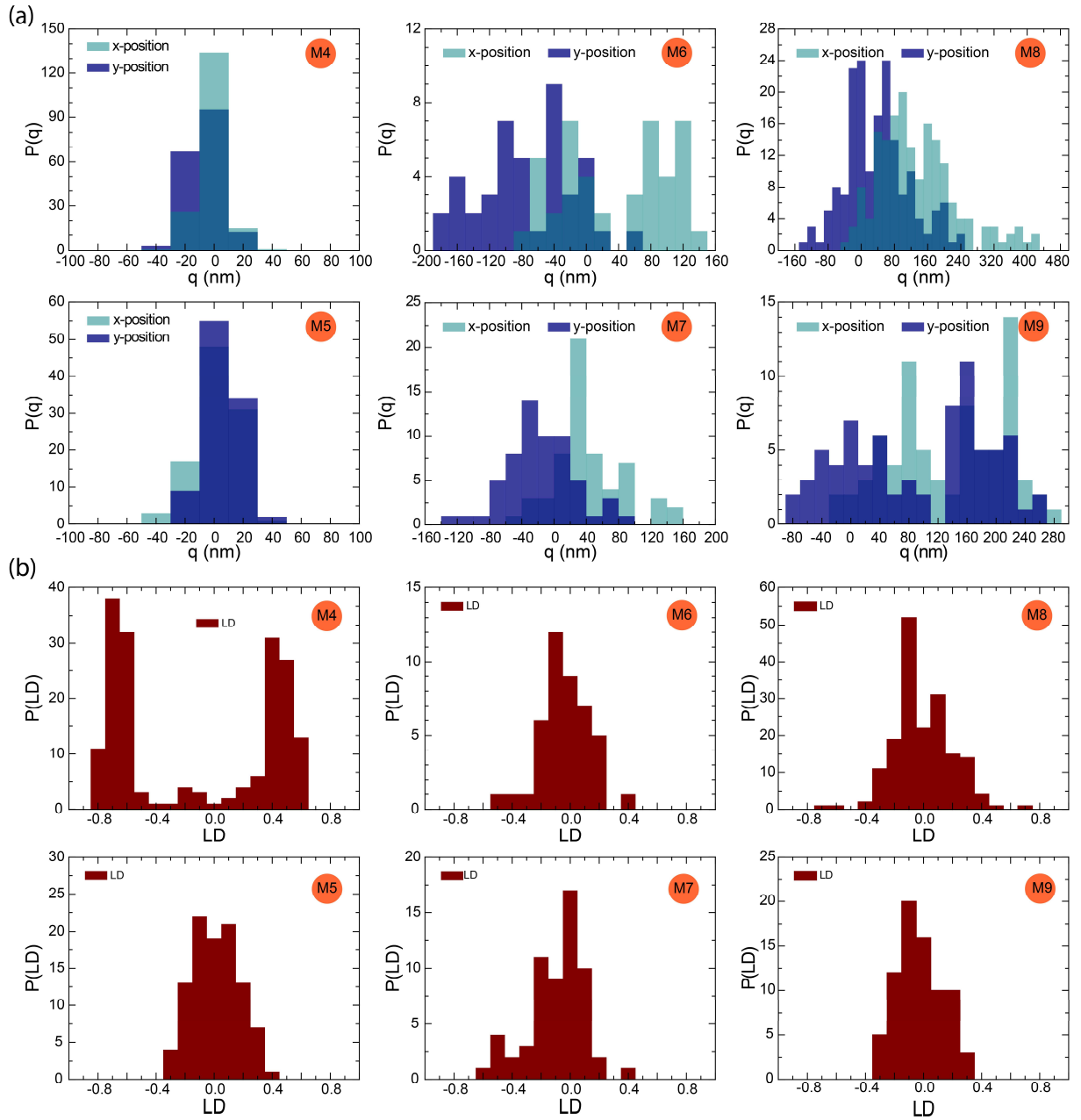


Fig. S6: Distribution of position ($\{x(t), y(t)\}$) and $LD(t)$ of the representative SM trajectories (M4-M9), which are used to discuss the three different dynamic scenarios, as shown in Fig. 3 of the main manuscript.

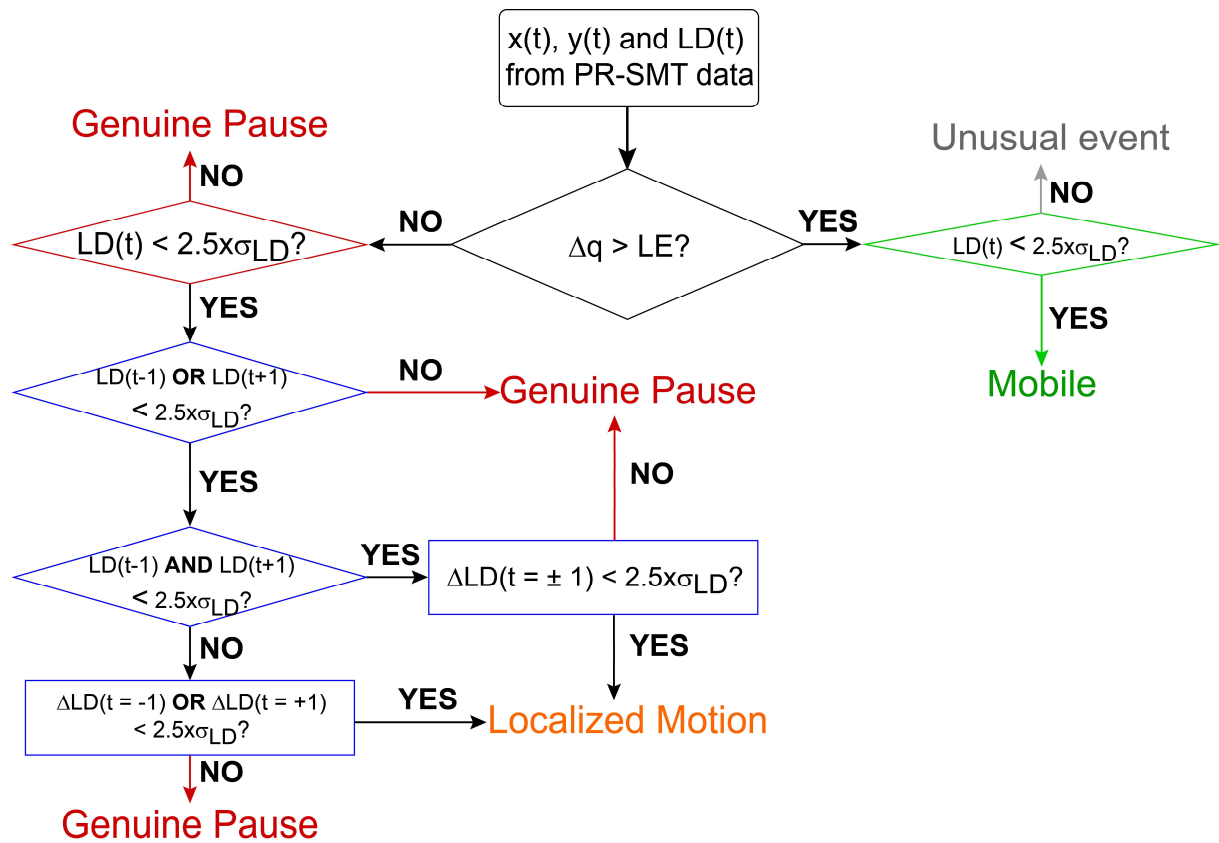


Fig. S7. The layout of the algorithm used to analyze the PR-SMT data. The translational movement within the LE is encoded as yellow color while the authentic immobile instances by red color. A clear translational movement is assigned green; however, a rare event where displacements are beyond LE and $LD(t)$ is beyond $2.5 \times \sigma_{LD}$ is encoded as grey.

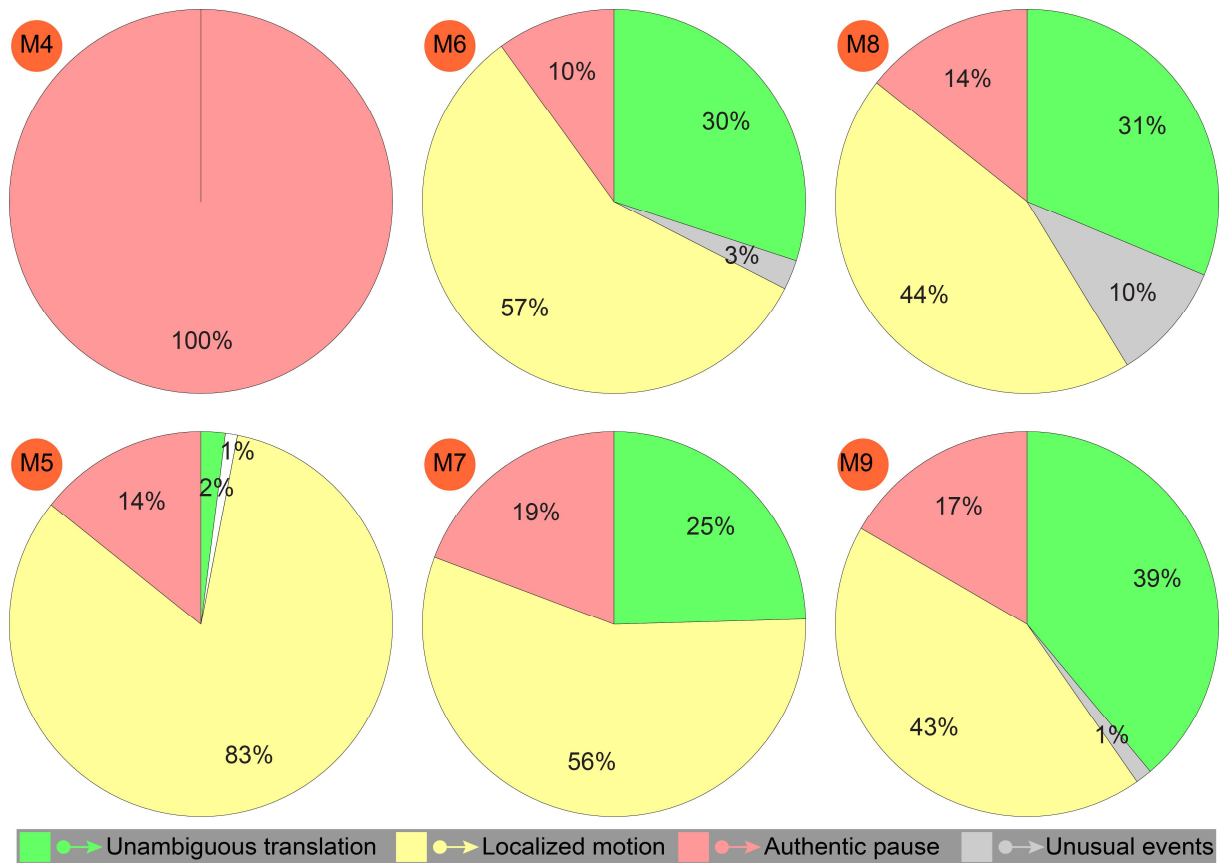


Fig. S8: The percentage of different dynamical events obtained from the PR-SMT analysis (Fig. 7) experienced by the representative tracers (M4-M9) is shown as pie charts. The bottom annotation represents the meaning of each used color.

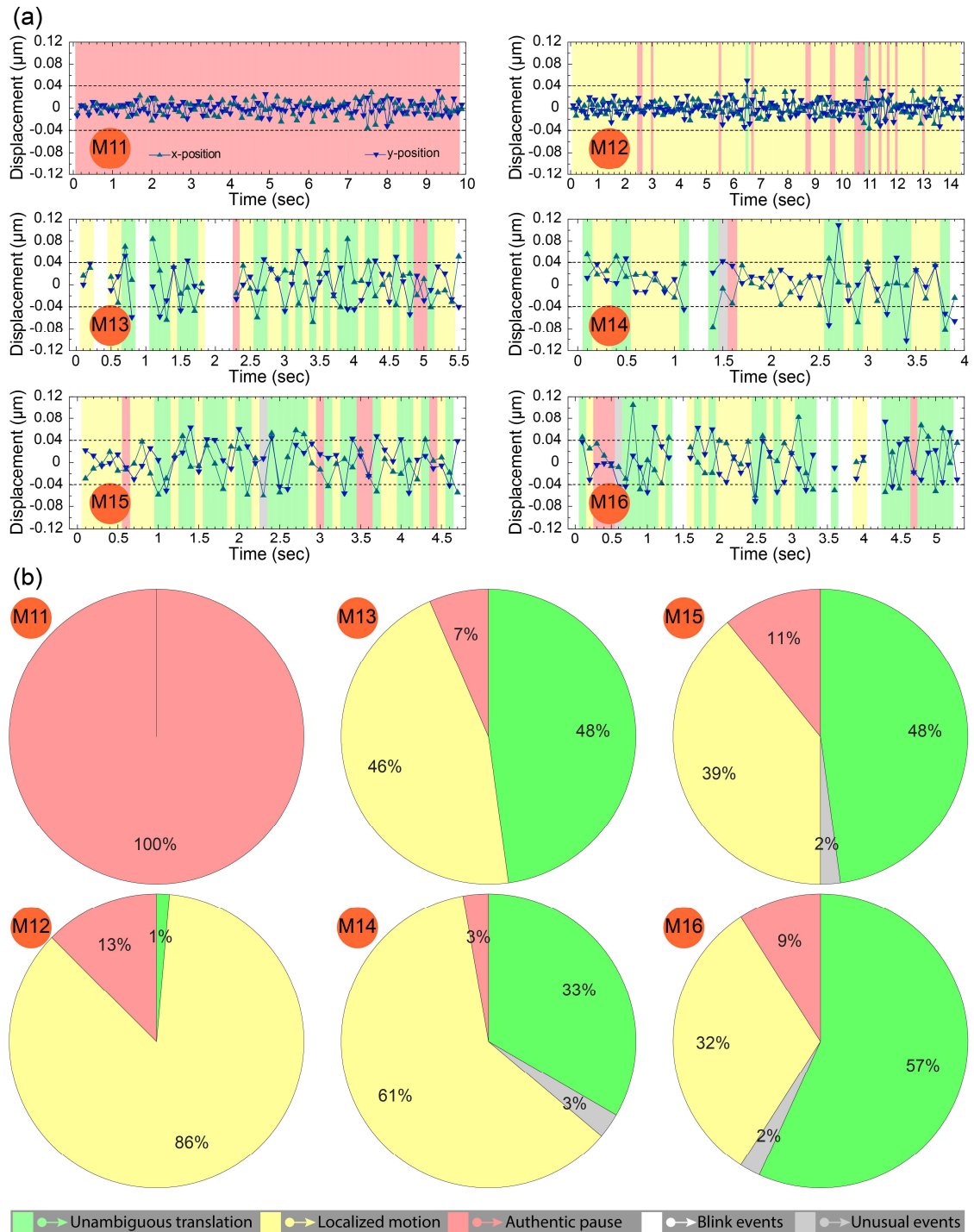


Fig. S9: Diverse dynamics as experienced by the six additional representative molecular tracers (M11-M16) during the transport. The annotated text at the bottom of each image represents each tracer's instantaneous dynamics and has the same meaning as Fig. 4 in the main manuscript. The bottom panel shows each dynamical events' corresponding percentage as a pie chart for the same molecules.

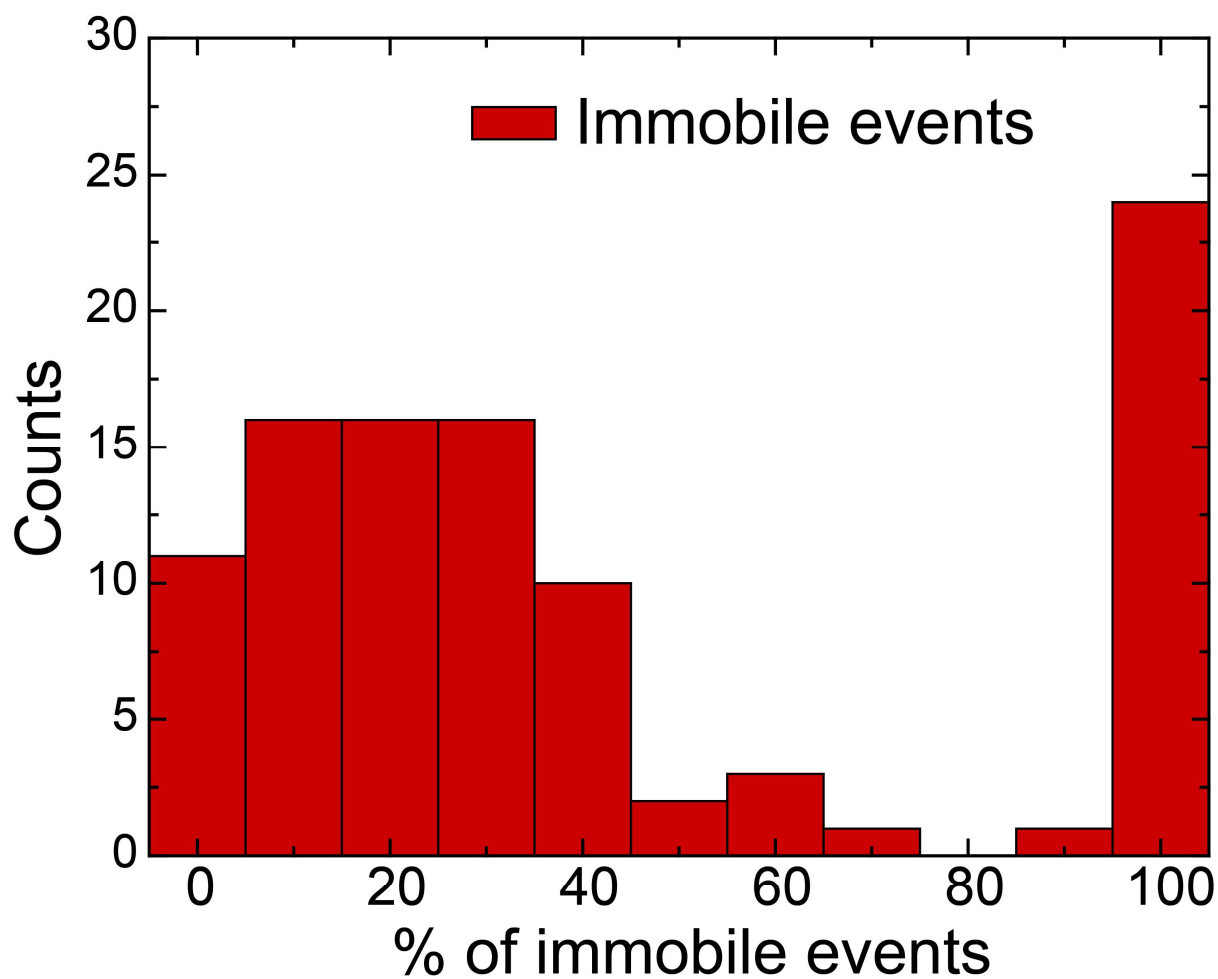


Fig. S10: The distribution of the percentage of immobile events as extracted from PR-SMT analysis for 100 SM tracers in the hydrated PVP matrix. The inset of Fig. 5a in the main manuscript was constructed using this distribution of % of immobile events.

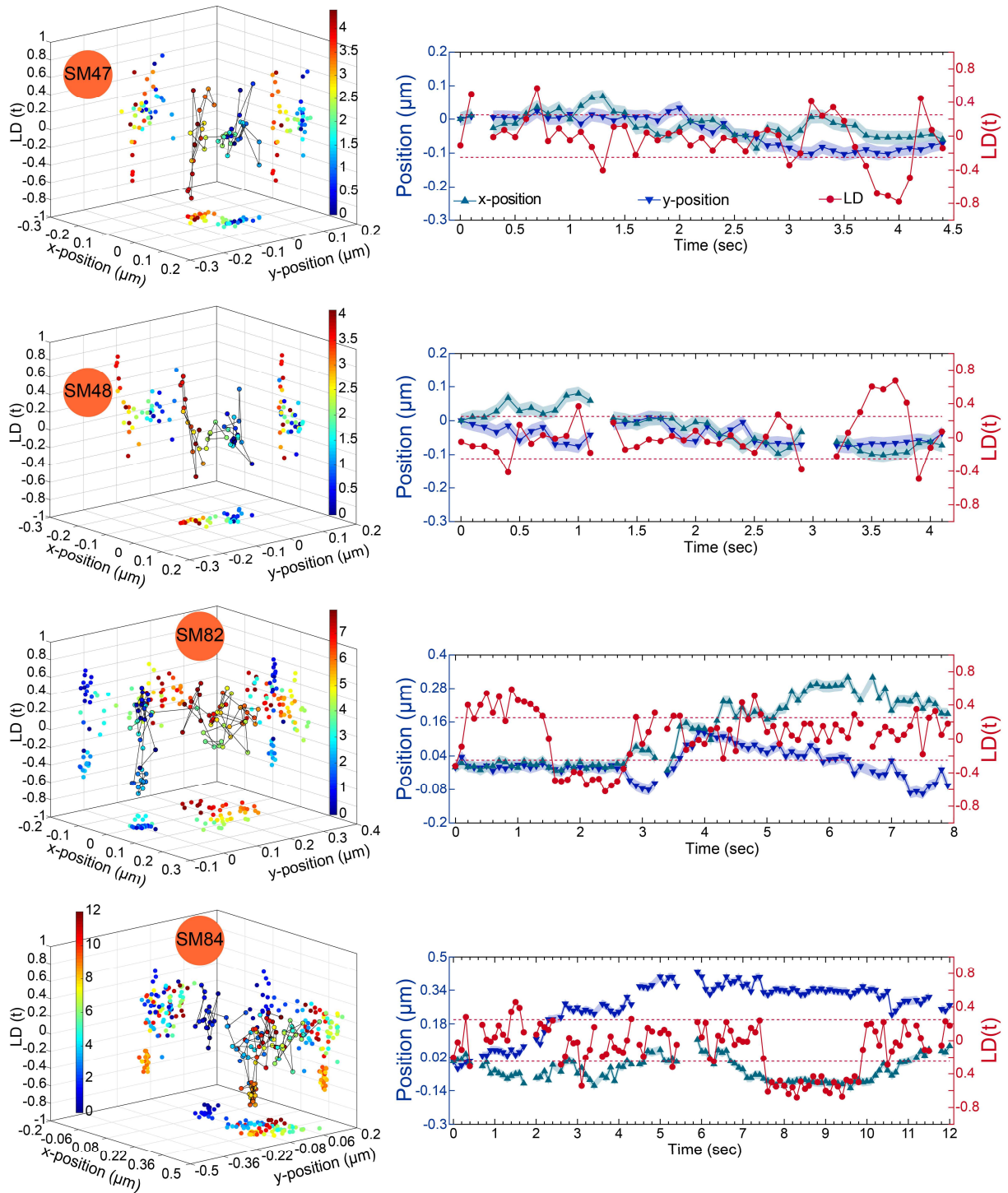


Fig. S11: The scatter plot and the temporal trajectory of position $\{x(t), y(t)\}$ and $LD(t)$ of four representative molecules where the tracer remains immobile for an extended duration during the transport. SM47 and SM48 are from each *Cat II*, while SM82 and SM 84 are from *Cat III*.

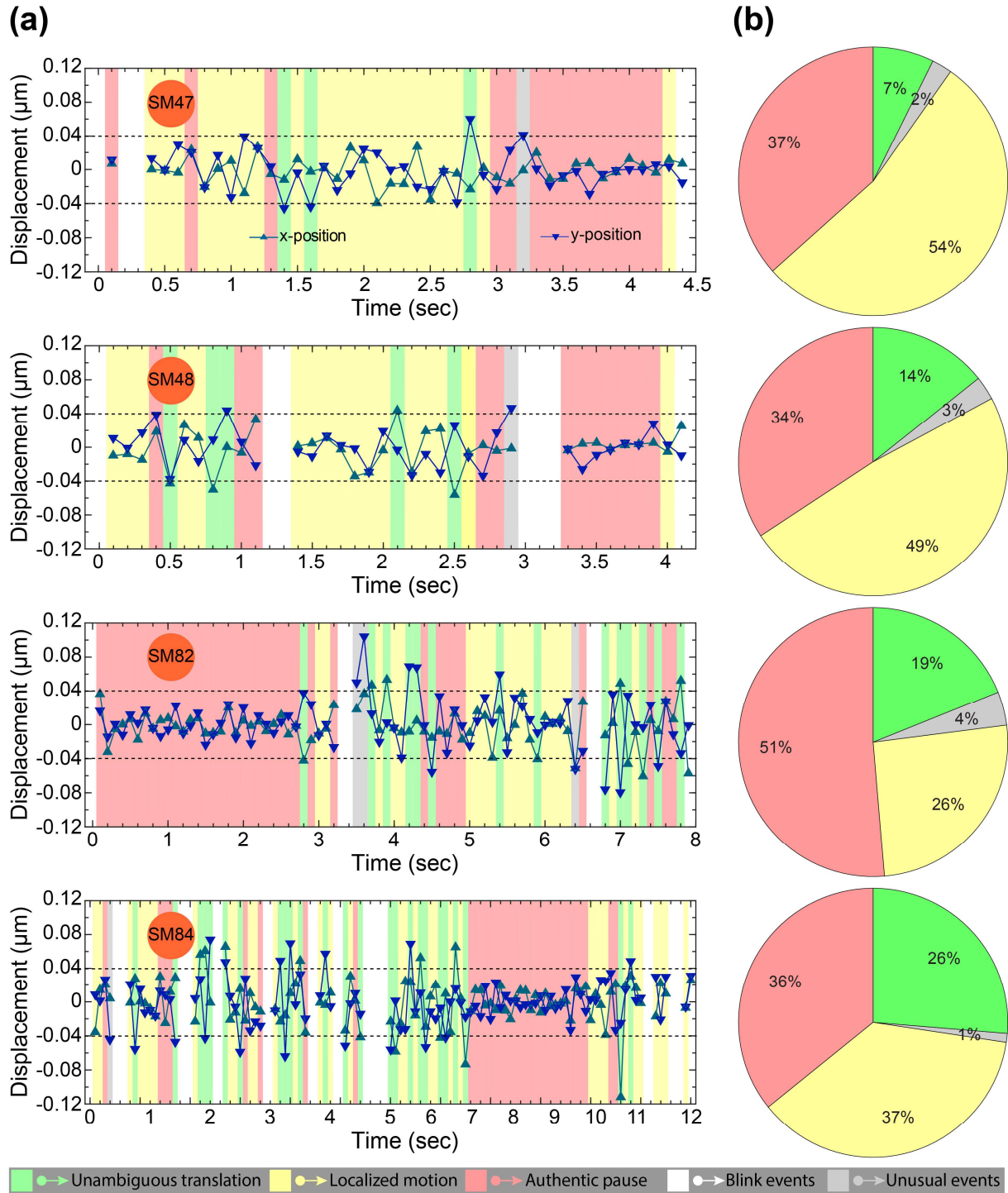


Fig. S12: (a) Diverse dynamical situation as experienced by the four representative tracers, which are immobile for a significant duration during the transport. (b) Pie chart of the percentage of each dynamic event. The bottom annotated text represents the meaning of each color.

Supplementary References

- 1 S. Bhattacharya, D. K. Sharma, S. Saurabh, S. De, A. Sain, A. Nandi and A. Chowdhury, Plasticization of poly(vinylpyrrolidone) thin films under ambient humidity: Insight from single-molecule tracer diffusion dynamics, *J. Phys. Chem. B*, 2013, **117**, 7771–7782.
- 2 M. W. Holman, R. Liu, L. Zang, P. Yan, S. A. DiBenedetto, R. D. Bowers and D. M. Adams, Studying and switching electron transfer: From the ensemble to the single molecule, *J. Am. Chem. Soc.*, 2004, **126**, 16126–16133.
- 3 S. Bhattacharya, D. K. Sharma, S. De, J. Mahato and A. Chowdhury, Heterogeneity during Plasticization of Poly(vinylpyrrolidone): Insights from Reorientational Mobility of Single Fluorescent Probes, *J. Phys. Chem. B*, 2016, **120**, 12404–12415.
- 4 L. C. C. Elliott, M. Barhoum, J. M. Harris and P. W. Bohn, Single molecule tracking studies of lower critical solution temperature transition behavior in poly(N-isopropylacrylamide), *Langmuir*, 2011, **27**, 11037–11043.
- 5 N. Tomczak, R. A. L. Vallée, E. M. H. P. van Dijk, M. García-Parajó, L. Kuipers, N. F. van Hulst and G. Julius Vancso, Probing polymers with single fluorescent molecules, *Eur. Polym. J.*, 2004, **40**, 1001–1011.
- 6 X. Michalet, Mean square displacement analysis of single-particle trajectories with localization error: Brownian motion in an isotropic medium, *Phys. Rev. E - Stat. Nonlinear, Soft Matter Phys.*, 2010, **82**, 041914–041926.
- 7 J. Enderlein, E. Toprak and P. R. Selvin, Polarization effect on position accuracy of fluorophore localization, *Opt. Express*, 2006, **14**, 8111–8120.
- 8 M. D. Lew, M. P. Backlund and W. E. Moerner, Rotational mobility of single molecules affects localization accuracy in super-resolution fluorescence microscopy, *Nano Lett.*, 2013, **13**, 3967–3972.
- 9 J. Engelhardt, J. Keller, P. Hoyer, M. Reuss, T. Staudt and S. W. Hell, Molecular orientation affects localization accuracy in superresolution far-field fluorescence microscopy, *Nano Lett.*, 2011, **11**, 209–213.